arXiv:1403.6133v1 [cond-mat.mtrl-sci] 24 Mar 2014

Shape Memory Alloy Nanostructures With Coupled Dynamic Thermo-Mechanical Effects

R. Dhote[1,3], H. Gomez[2], R. Melnik[3], J. Zu[1]
[1]Mechanical and Industrial Engineering, University of Toronto,
5 King's College Road, Toronto, ON, M5S3G8, Canada
[2]Department of Applied Mathematics, University of A Coruña
Campus de Elvina, s/n. 15192 A Coruña, Spain
[3]M[2]NeT Laboratory, Wilfrid Laurier University, Waterloo, ON, N2L3C5, Canada

Abstract: Employing the Ginzburg-Landau phase-field theory, a new coupled dynamic thermo-mechanical 3D model has been proposed for modeling the cubic-to-tetragonal martensitic transformations in shape memory alloy (SMA) nanostructures. The stress-induced phase transformations and thermo-mechanical behavior of nanostructured SMAs have been investigated. The mechanical and thermal hysteresis phenomena, local non-uniform phase transformations and corresponding non-uniform temperature and deformations distributions are captured successfully using the developed model. The predicted microstructure evolution qualitatively matches with the experimental observations. The developed coupled dynamic model has revealed a better understanding of underlying martensitic transformation mechanisms in SMAs, as well as their effect on the thermo-mechanical behavior of nanostructures.

1 Introduction

Shape memory alloys (SMAs) exhibit a remarkable behavior that arises from an interplay between microstructures in two phases, a high temperature symmetric austenite and low temperature symmetric martensite phases via martensitic transformations (MTs). The complex non-uniform and temperature dependent microstructure morphology results in surface relief [1] and domain pattern [2] formations due to elastic deformations (or strains) under temperature or stress induced loadings. Furthermore, the ability to control deformations in different geometries and loading conditions can lead to tailoring of mechanical structures [3] for better SMA-based actuator and sensors in NEMS, MEMS and biomedical applications [4, 5, 6, 7, 8, 9]. The ability to control strain is also essential for ferroic materials and semiconductor devices. For instance, widely studied, optical response properties in low-dimensional semiconductor nanostructures [10] and behavior of ferroelectric materials in FeRAMs [11] can be better understood by incorporating coupled thermo-mechanical effects in a physics-based model. Indeed, since SMAs have temperature dependent microstructures and properties, in order to control deformations in a structure, it is highly relevant to study the morphology of complex 3D martensitic twins, as a function of temperature.

Recently, MTs have been studied by using atomistic simulations [12]. Simulating larger domains at submicron scales requires enormous computational power which limits its use. In order to overcome this limitation, continuum descriptions at the submicron length scale have become an effective tool to model experimentally observed phenomena. One of the continuum based method is the phase-field (PF) approach that has been widely used to investigate qualitatively microstructures and underlying mechanisms in nanoferroic systems [13, 14]. Particularly, in the ferroelastic systems, the PF model has been implemented successfully to understand martensitic transformations in SMA nanostructures under isothermal [15] or athermal conditions [16]. The isothermal assumption particularly holds for quasistatic or slow strain rate loadings. However, the isothermal assumption is a strong hypothesis under a dynamic loading of SMAs as the phase transformation causes the temperature evolution due to self-heating or cooling of the system, consequently affecting their mechanical behavior, due to insufficient time for heat transfer to the environment as observed experimentally [17, 18]. Therefore, a theoretical framework that couples the

mechanical behavior with temperature evolution is imperative to describe the MTs and their behavior in SMA nanostructures for critical application developments.

2 Mathematical Model

For the first time, we develop and apply a fully coupled dynamic thermo-mechanical 3D PF model to the investigation of the stress-induced phase transformations and behavior in SMA nanostructures. The cubic-to-tetragonal PT is described by deviatoric strains defined in terms of symmetry adapted combinations of the components of the strain tensor. The model is developed based on the Ginzburg-Landau theory. The physical domain is parametrized by Cartesian coordinates $\boldsymbol{x} = \{x_1, x_2, x_3\}^T$. The Cauchy-Lagrange infinitesimal symmetric strain tensor $\boldsymbol{\epsilon}$ can be defined in components as $\epsilon_{ij} = (u_{i,j} + u_{j,i})/2$, $i, j \in \{1, 2, 3\}$, where an inferior comma denotes partial differentiation (e.g., $u_{i,j} = \partial u_i / \partial x_j$) and $\boldsymbol{u} = \{u_1, u_2, u_3\}^T$ is the displacement field. The symmetric strains e_i for the cubic-to-tetragonal phase transformation can be defined as $e_1 = 1/\sqrt{3}(\epsilon_{11} + \epsilon_{22} + \epsilon_{33})$, $e_2 = 1/\sqrt{2}(\epsilon_{11} - \epsilon_{22})$, $e_3 = 1/\sqrt{6}(\epsilon_{11} + \epsilon_{22} - 2\epsilon_{33})$, $e_4 = \epsilon_{23}$, $e_5 = \epsilon_{13}$, $e_6 = \epsilon_{12}$, where e_1 is the hydrostatic strain, e_2, e_3 are the deviatoric strains, and e_4, e_5 and e_6 are the shear strains.

We use the symmetric strain based free energy functional, for cubic-to-tetragonal phase transformations, initially proposed by Barsch et al. [19] and later modified by Ahluwalia et al. [15] to study the martensitic transformations in SMA nanostructures. The free energy functional $\mathscr{F}$ with anharmonic components of OPs and harmonic components of non-OP components is expressed as

$$\mathscr{F}[\boldsymbol{u}] = \int_\Omega \left[F_0(e_i) + \frac{k_g}{2} \left(|\nabla e_2|^2 + |\nabla e_3|^2 \right) \right] \mathrm{d}\Omega, \tag{1}$$

where F_0 is defined as

$$F_0(e_i) \;\; = \frac{a_1}{2} e_1^2 + \frac{a_2}{2} \left(e_4^2 + e_5^2 + e_6^2 \right) + a_3 \tau \left(e_2^2 + e_3^2 \right) + a_4 e_3 \left(e_3^2 - 3 e_2^2 \right) + a_5 (e_2^2 + e_3^2)^2. \tag{2}$$

Here a_i, $(i = 1, \ldots, 5)$ and k_g are material parameters, τ is the dimensionless temperature coefficient defined as $\tau = (\theta - \theta_m)/(\theta_0 - \theta_m)$, where θ_0 and θ_m are the material properties specifying the transformation start and end temperatures, and $|\cdot|$ in (1) denotes the Euclidean norm of a vector (that is $|\nabla e_k| = (\partial e_k / \partial x_i)^2$, where k = 2 or 3).

The deviatoric strains are selected as the order-parameters (OPs) to describe different phases in the domain Ω. Using these notations, and the repeated-indices summation convention, our model can be written as

$$\rho \ddot{u}_i \;\; = \sigma_{ij,j} + \eta \sigma'_{ij,j} + \mu_{ij,kkj} + f_i, \tag{3a}$$

$$C_v \dot{\theta} \;\; = \kappa \theta_{,ii} + \Xi \theta \left(u_{i,i} \dot{u}_{j,j} - 3 u_{i,i} \dot{u}_{i,i} \right) + g, \tag{3b}$$

where a dot over a function denotes partial differentiation with respect to time, ρ, η, C_v, κ, and Ξ are positive constants that represent, respectively, the density, viscous dissipation, specific heat, thermal conductance coefficient, and strength of the thermo-mechanical coupling. The symmetric stress tensor defined as $\boldsymbol{\sigma} = \{\sigma_{ij}\} = \partial \mathscr{F} / \partial \epsilon_{ij}$, is a nonlinear function of the strain measures and the temperature coefficient τ. The dissipation stress tensor has the form $\boldsymbol{\sigma'} = \{\sigma'_{ij}\} = \partial \mathscr{R} / \partial \epsilon'_{ij}$, where the Rayleigh dissipation is defined as $\mathscr{R}[\dot{\boldsymbol{u}}] = \int_\Omega \eta/2 |\dot{\boldsymbol{\epsilon}}|^2 \, \mathrm{d}\Omega$.

The second-rank tensor $\boldsymbol{\mu} = \{\mu_{ij}\}$, the microstress tensor, is a non-symmetric tensor defined as $\boldsymbol{\mu} = \frac{k_g}{3} \left(\nabla^T \boldsymbol{u} - 3 \nabla_d \boldsymbol{u} \right)$, where k_g is a positive constant, $\nabla^T \boldsymbol{u}$ denotes the transpose of the displacement gradient (i.e., $\nabla^T \boldsymbol{u} = \{u_{j,i}\}$), and $\nabla_d \boldsymbol{u} = \mathrm{diag}(u_{1,1}, u_{2,2}, u_{3,3})$, where $\mathrm{diag}(a, b, c)$ is a 3×3 diagonal matrix whose diagonal entries starting in the upper left corner are a, b, c. Finally, $\boldsymbol{f} = \{f_1, f_2, f_3\}^T$ and g represent, respectively, mechanical and thermal loads.

The simulations were performed for homogeneous single crystal FePd rectangular prism nanowire of dimension 160×40×40 nm. The material properties used during the simulations are [13, 20]:
a_1= 192.3 GPa, a_2= 280 GPa, a_3= 19.7 GPa, a_4= 2.59× 10^3 GPa, a_5= 8.52× 10^4 GPa, $k_g = 3.5 \times 10^{-8}$ N, $\theta_{\text{init}} = 250$ K, $\theta_{\text{m}} = 270$ K, $\theta_0 = 295$ K, $C_v = 350$ Jkg^{-1}K^{-1}, $\kappa = 78$ Wm^{-1}K^{-1}, and $\rho = 10000$ kg m^{-3}.

The governing equations Eqs. (3) are strongly thermo-mechanically coupled in a non-linear manner, with fourth-order differential terms. These complex equations are not amenable to a closed form solution. They pose great challenges to numerical approaches. We have developed an isogeometric analysis (IGA) [21] framework that allows the straightforward solution to the developed model. It also allows the use of coarser meshes, larger time steps along with geometrical flexibility and accuracy [22].

3 Numerical Simulations

To elucidate the capabilities of the developed model from physics point of view, the simulations have been conducted on a rectangular prism nanowire domain of dimension 160×40×40 nm (meshed with 162×42×42 uniform quadratic $\mathscr{C}^1$-continuous B-spline basis functions) to investigate its thermo-mechanical behavior subjected to dynamic stress-induced loadings. The simulations to examine the pseudoelastic (PE) and shape memory effect (SME) behavior of SMAs, as a function of microstructures, have been performed.

To study the PE behavior, the SMA nanowire is quenched to the dimensionless temperature corresponding to $\tau = 1.12$ and allowed to evolve starting from a random initial condition corresponding to displacement $\mathbf{u}$ and periodic boundary conditions. The nanowire has been evolved till the microstructure and free energy are stabilized. The nanowire remains in the austenite phase. The evolved microstructures are then axially loaded by mechanically constraining one end of the specimen $\mathbf{u} = \mathbf{0}$, and loading the opposite end using a ramp based displacement equivalent to the strain rate 3×10^7/s as shown in Fig. 1(o). Figure 1(a-g) shows different time snapshots of microstructure evolution during loading and the end of unloading cycle. The austenite (yellow) is converted into the favorable M_1 martensite (red) with the formation and migration of habit plane in the nanowire. At the end of unloading, the nanowire returns to the austenite phase (refer to Fig. 1(g)). The mechanical hysteresis, the average σ_{11}–ϵ_{11} (blue color), forms a full loop with zero remnant strain at the end of unloading. The temperature hysteresis, the average τ–ϵ_{11} (red color), indicates a global increase in the temperature during loading and a decrease during unloading as a result of exothermic and endothermic processes.

The phase transformation is a local phenomenon that leads to non-uniform deformation and temperature fields in the domain. The local variation of the non-dimensional temperature τ is presented as an arc-length extrusion plot along the central axis of the nanowire during loading and unloading in Fig. 1(i) . The non-uniform strain and deformation are apparent during phase transformations. The local increase in temperature, as observed in Figs 1(o) serves as a signature of formation or movement of habit planes as indicated in the inset. As the loading progresses, the heat produced is conducted in the domain causing self-heating thus increasing the global temperature. As the domain is small, the heat is conducted quickly causing small local peaks as compared to the experiments where large temperature peaks were observed in a big macro specimens [23].

To study the SME behavior, the SMA nanowire is quenched to the temperature corresponding to $\tau =$ -1.2 and allowing the microstructures and energy to stabilize. The nanowire domain is evolved into the accommodated twinned martensites with all three variants present in approximately equal proportions as shown in Fig. 2(a). Next, the evolved microstructures are axially loaded by mechanically constraining one end of the specimen $\mathbf{u} = \mathbf{0}$, and loading the opposite end using a ramp based displacement equivalent to the strain rate 3×10^7/s. The movement of domain walls, merging and elimination of unfavorable domains and growth of favorable ones are apparent. During loading, the accommodated twinned microstructures are transformed into a detwinned microstructure via a phase transformation of unfavorable M_2 (blue) and

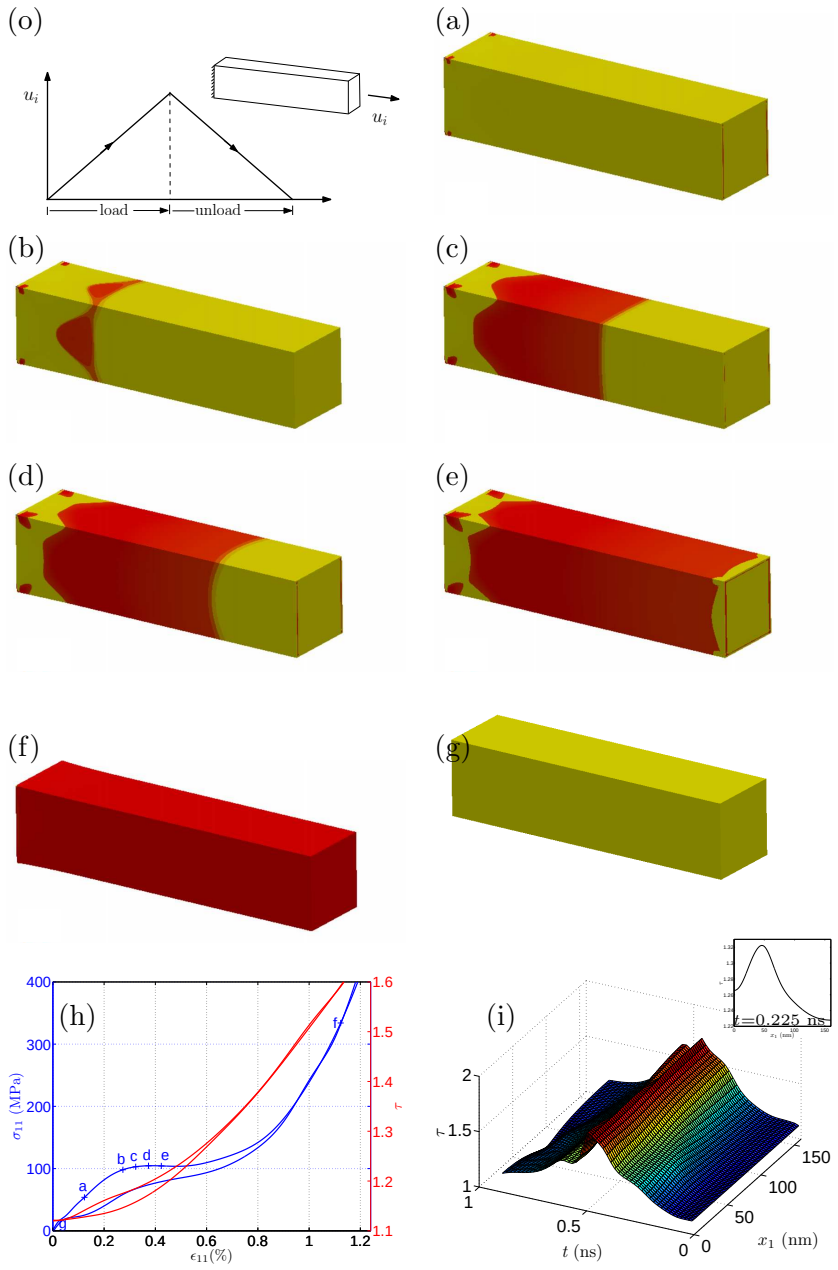

Figure 1: Pseudoelasticity: Subplots (a-g) show the microstructure morphology evolution during loading and unloading (red and yellow colors represent M_1 variant and austenite phase). Hysteresis plots of average $\sigma_{11} - \epsilon_{11}$ (blue) and $\tau - \epsilon_{11}$ (red) are shown in subplot (h). Time extrusion plot of average τ over the arc-length along the center line of the rectangular prism (between the opposite ends (0,20,20)–(160,20,20) nm) is shown in subplot (i). The schematic of loading-unloading cycle is shown in subplot (o).

M_3 (green) variants to the favorable M_1 martensite (red). The domain walls migrate along [110] planes. On unloading, the nanowire still exists in M_1 phase at axial stress in the domain being zero (refer to Fig. 2(h)). The nanowire is then unloaded to zero stress-strain configuration with the same strain rate but now by applying external heat $g = 0.1$ (in the dimensionless units). The nanowire is converted to the austenite phase forming a full-SME loop.

The local variation of non-dimensional temperature τ is presented as an arc-length extrusion plot in Fig. 2(j). The non-uniform strain and deformation is apparent during phase transformations. The local deformation is non-uniform during loading and it becomes nearly uniform after all the unfavorable variants are converted to the favorable ones. The local increase in temperature at one time instant is indicated in the inset. As the loading progresses, the heat produced is conducted in the domain causing self-heating thus increasing the global temperature. The model qualitatively captures this local phenomenon [18, 17].

The developed model has enabled us to capture the inherent temperature hysteresis qualitatively, which is in agreement with the experiments [18]. The model has also successfully captured thermal hysteresis τ–ϵ_{11} in the PE and the complete σ_{11}–ϵ_{11}–τ loop in SME. Under the dynamic loading conditions of SMA nanowires, this has been done for the first time.

4 Nanoscale Dynamics of Spring

To the best of our knowledge, we first report the simulations results on a complex nanostrucutred SMA tubular spring specimen using the phase-field model. A two loop spring has the pitch of 190 nm and mean diameter of 60 nm. The outer and inner diameters of the tube are 82.5 nm and 41.25 nm. The tubular spring is meshed with 134, 16, and 266 $\mathscr{C}^1$-quadratic NURBS basis functions in circumferential, radial, and helix directions, respectively. The top end of the SMA spring specimen is elastically loaded in x_2 direction and the bottom end is constrained with $\boldsymbol{u} = \boldsymbol{0}$. The spring is consecutively loaded for two ramp loading-unloading cycles, each with 3 % displacement with strain rate equivalent to 3×10^7/s. The microstructures during the first and second cycles, at the same deformation (u_2 displacement), are presented in Figs. 3(a-f) and 3(a′-f′) respectively. The microstructure morphology is different at the same deformation of the spring during the two consecutive cycles. The study demonstrates the influence of dynamic loading on a microstructure evolution.

The developed model can be modified in a straightforward manner to incorporate the size dependent properties in the nanoscale specimens. Such accurate models can enhance our understanding of the MTs and thermo-mechanical behaviors of SMA nanostructures and provide guidelines for better device and application development.

5 Conclusions

A new fully coupled thermo-mechanical 3D PF model has been developed that captures underlying response of SMA nanostructures. It also qualitatively captures the important features of mechanical and thermal hystereses in pseudoelastic and shape memory effect during stress-induced transformations. The temperature variation during loading and unloading of SMA nanowire due to exothermic and endothermic processes has been successfully captured as well. The local temperature distribution acts as a signature of formation or movement of habit plane or domain wall. The model provides important information for better understanding of the MT mechanisms under dynamic loading conditions in SMA nanowires.

References

[1] M. Wu, W. Huang, Y. Fu, F. Chollet, Y. Hu, and M. Cai. Reversible surface morphology in shape-memory alloy thin films. *Journal of Applied Physics*, 105(3):033517–033517, 2009.

[2] K. Bhattacharya. *Microstructure and Martensite: Why it Forms and how it Gives Rise to the Shape-memory Effect*, volume 2. Oxford University Press, 2003.

[3] K. Bhattacharya and R. James. The material is the machine. *Science*, 307(5706):53–54, 2005.

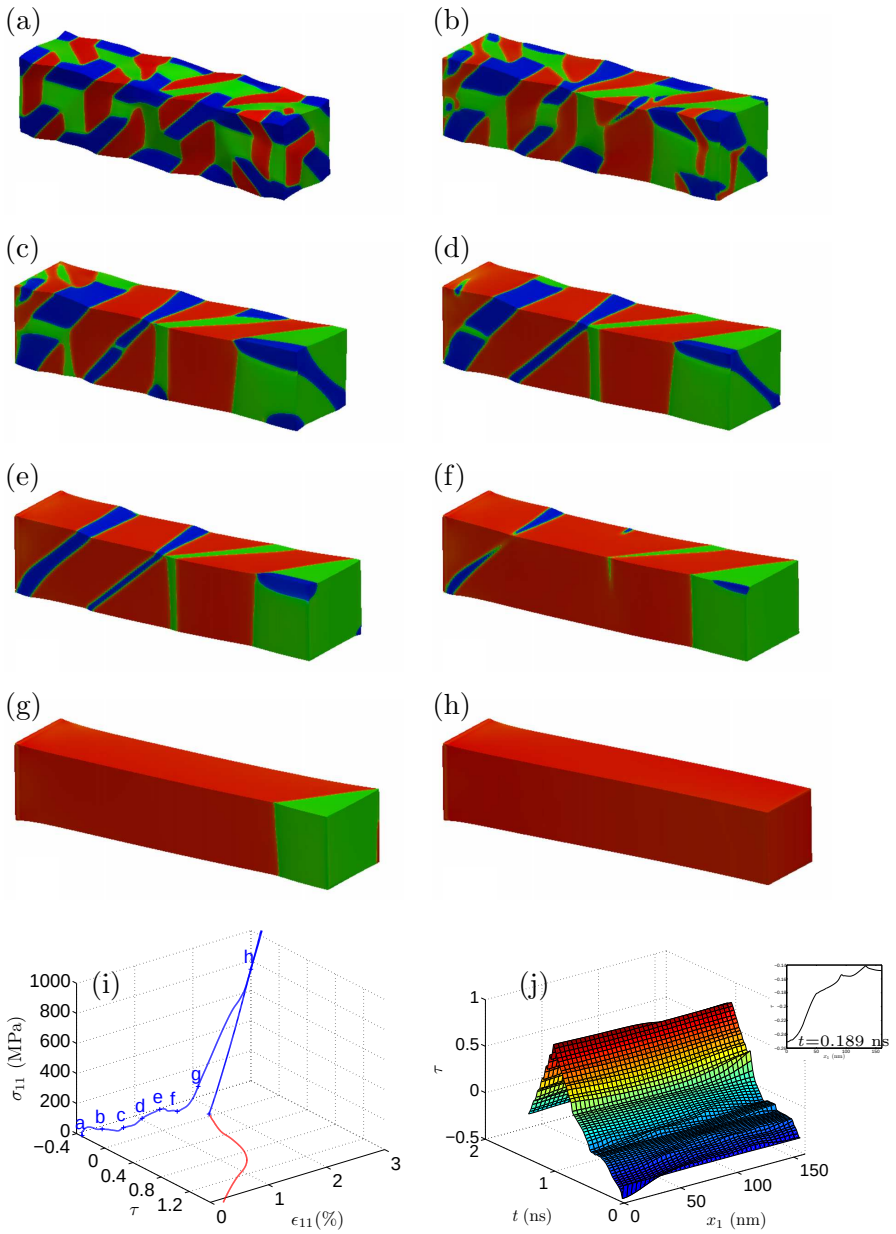

Figure 2: Shape memory effect: Subplots (a-h) show the microstructure morphology evolution during loading and unloading (red, blue, and green colors represent M_1, M_2, and M_3 variants, respectively). The full SME loop behavior is shown in subplot (h) (red color indicate heating part of the cycle) . Time extrusion plot of average τ over the arc-length along the center line of the rectangular prism (between the opposite ends (0,20,20)–(160,20,20) nm) is shown in subplot (i).

[4] K. Žužek Rožman, D. Pečko, S. Šturm, U. Maver, P. Nadrah, M. Bele, and S. Kobe. Electrochemical synthesis and characterization of $Fe_{70}Pd_{30}$ nanotubes for drug-delivery applications. *Materials Chemistry and Physics*, 133(1):218–224, 2012.

[5] D. König, M. Ehmann, S. Thienhaus, and A. Ludwig. Micro-to nanostructured devices for the characterization of scaling effects in shape-memory thin films. *Journal of Microelectromechanical Systems*, 19(5):1264–1269, 2010.

[6] B. Bayer, S. Sanjabi, C. Baehtz, C. Wirth, S. Esconjauregui, R. Weatherup, Z. Barber, S. Hofmann,

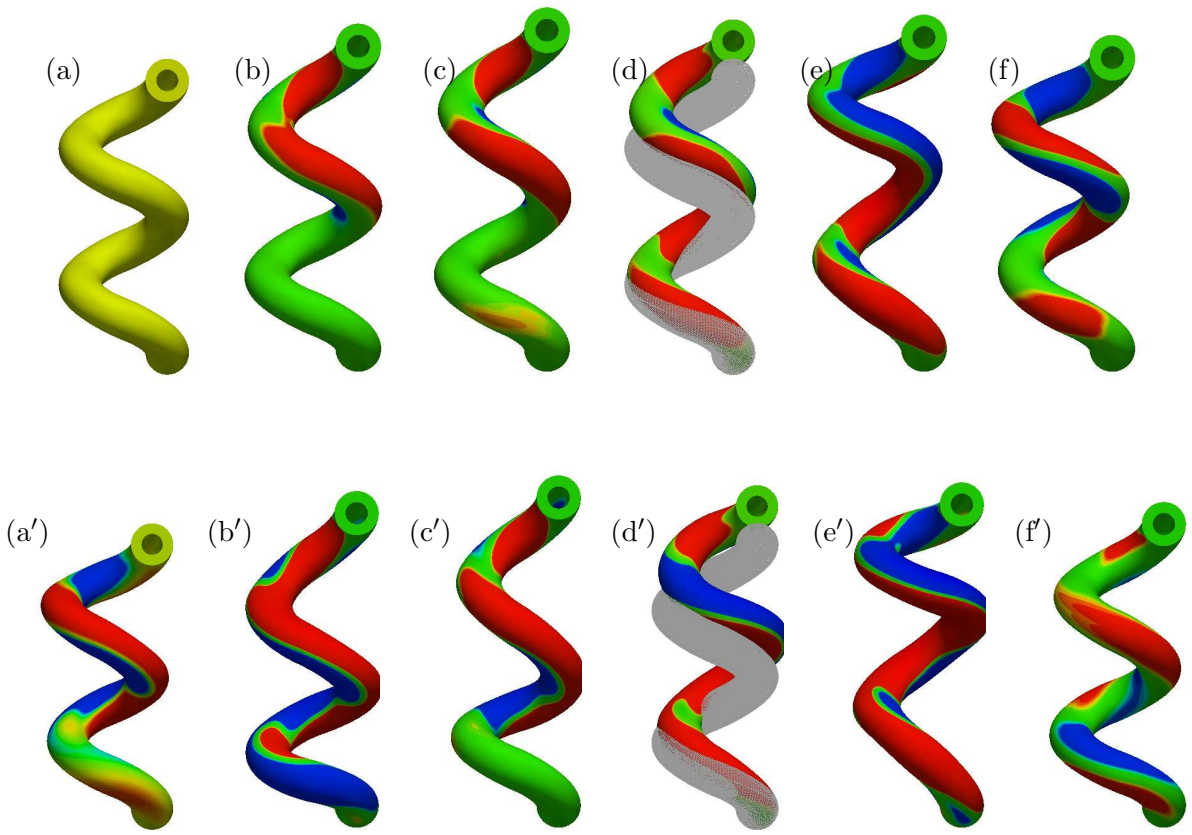

Figure 3: Microstructure evolution during pseudoelastic loading of a tubular nanostructured spring for two ramp loading-unloading cycles: a-f show the first cycle, a′-f′ the second cycle (yellow, red, blue, and green colors represent austenite, M_1, M_2, and M_3 variants, respectively). The grey color represent undeformed mesh at the end of loadings in d and d′.

and J. Robertson. Carbon nanotube forest growth on NiTi shape memory alloy thin films for thermal actuation. *Thin Solid Films*, 519(18):6126–6129, 2011.

[7] Manfred Kohl. *Shape memory microactuators*. Springer, 2004.

[8] S. Miyazaki, Y. Fu, and W. Huang. *Thin film shape memory alloys: fundamentals and device applications*. Cambridge University Press, 2009.

[9] T. Yoneyama and S. Miyazaki. *Shape memory alloys for biomedical applications*. CRC Press, 2009.

[10] S. Prabhakar and R. Melnik. Influence of electromechanical effects and wetting layers on band structures of AlN/GaN quantum dots and spin control. *Journal of Applied Physics*, 108:064330, 2010.

[11] J. Scott. Applications of modern ferroelectrics. *Science*, 315(5814):954–959, 2007.

[12] Y. Zhong, K. Gall, and T. Zhu. Atomistic study of nanotwins in NiTi shape memory alloys. *Journal of Applied Physics*, 110(3):033532–033532, 2011.

[13] M. Bouville and R. Ahluwalia. Microstructure and Mechanical Properties of Constrained Shape Memory Alloy Nanograins and Nanowires. *Acta Mater.*, 56(14):3558–3567, 2008.

[14] N. Ng, R. Ahluwalia, and D.J. Srolovitz. Domain patterns in free-standing nanoferroelectrics. *Acta Materialia*, 60(8):3632–3642, 2012.

[15] R. Ahluwalia, T. Lookman, and A. Saxena. Dynamic Strain Loading of Cubic to Tetragonal Martensites. *Acta Materialia*, 54:2109–2120, 2006.

[16] V. Levitas and D. Lee. Athermal resistance to interface motion in the phase-field theory of microstructure evolution. *Physical review letters*, 99(24):245701, 2007.

[17] J. Shaw and S. Kyriakides. On the nucleation and propagation of phase transformation fronts in a niti alloy. *Acta Materialia*, 45(2):683–700, 1997.

[18] E. Pieczyska, S. Gadaj, W. Nowacki, and H. Tobushi. Phase-transformation fronts evolution for stress-and strain-controlled tension tests in tini shape memory alloy. *Experimental Mechanics*, 46(4):531–542, 2006.

[19] G. Barsch and J. Krumhansl. Twin Boundaries in Ferroelastic Media without Interface Dislocations. *Phys. Rev. Lett.*, 53(11):1069–1072, Sep 1984.

[20] S. Kartha, J. A. Krumhansl, J. P. Sethna, and L. K. Wickham. Disorder-driven pretransitional tweed pattern in martensitic transformations. *Phys. Rev. B Condens. Matter.*, 52(2):803–822, 07 1995.

[21] C. J. Austin, T.J.R. Hughes, and Y. Bazilevs. *Isogeometric Analysis: Toward Integration of CAD and FEA*. John Wiley & Sons., 2009.

[22] R. Dhote, H. Gomez, R. Melnik, and J. Zu. 3d coupled thermo-mechanical phase-field modeling of shape memory alloy dynamics via isogeometric analysis. *Computer Methods in Applied Mechanics and Engineering*, 2014. (submitted).

[23] J.A. Shaw and S. Kyriakides. Thermomechanical aspects of niti. *Journal of the Mechanics and Physics of Solids*, 43(8):1243–1281, 1995.